Published OnlineFirst July 16, 2013; DOI: 10.1158/2159-8290.CD-13-0330

RESEARCH BRIEF

SF3B1 Mutations Are Associated with Alternative Splicing in Uveal Melanoma

Simon J. Furney[1], Malin Pedersen[2], David Gentien[3,6], Amaury G. Dumont[6,7], Audrey Rapinat[3,6], Laurence Desjardins[4,6], Samra Turajlic[2], Sophie Piperno-Neumann[5,6], Pierre de la Grange[8], Sergio Roman-Roman[6,7], Marc-Henri Stern[3,6], and Richard Marais[1]

ABSTRACT

Uveal melanoma, the most common eye malignancy, causes severe visual morbidity and is fatal in approximately 50% of patients. Primary uveal melanoma can be cured by surgery or radiotherapy, but the metastatic disease is treatment refractory. To understand comprehensively uveal melanoma genetics, we conducted single-nucleotide polymorphism arrays and whole-genome sequencing on 12 primary uveal melanomas. We observed only approximately 2,000 predicted somatic single-nucleotide variants per tumor and low levels of aneuploidy. We did not observe an ultraviolet radiation DNA damage signature, but identified *SF3B1* mutations in three samples and a further 15 mutations in an extension cohort of 105 samples. *SF3B1* mutations were associated with good prognosis and were rarely coincident with *BAP1* mutations. *SF3B1* encodes a component of the spliceosome, and RNA sequencing revealed that *SF3B1* mutations were associated with differential alternative splicing of protein coding genes, including *ABCC5* and *UQCC*, and of the long noncoding RNA *CRNDE*.

SIGNIFICANCE: Our data show that despite its dismal prognosis, uveal melanoma is a relatively simple genetic disease characterized by recurrent chromosomal losses and gains and a low mutational burden. We show that *SF3B1* is recurrently mutated in uveal melanoma, and the mutations are associated with aberrant alternative splicing. *Cancer Discov; 3(10); 1122–9. ©2013 AACR.*

INTRODUCTION

Uveal melanoma arises in the iris, ciliary body, and choroid. Light skin complexion, fair hair, blue eyes, and the presence of cutaneous nevi are risk factors in uveal melanoma (1), but the ultraviolet radiation (UVR)-associated increase in cutaneous melanoma that has occurred in countries such as Australia over the past 4 decades has not been accompanied by parallel increases in uveal melanoma (2–4). Thus, the role of UVR in uveal melanoma etiology is unclear.

Authors' Affiliations: [1]The Cancer Research UK Manchester Institute, Manchester; [2]The Institute of Cancer Research, London, United Kingdom; [3]Platform of Molecular Biology Facilities, Translational Research Department and Departments of [4]Ophthalmological Surgery and [5]Medical Oncology, [6]Institut Curie; [7]INSERM U830; and [8]GenoSplice, Hopital Saint-Louis, Paris, France

Note: Supplementary data for this article are available at Cancer Discovery Online (http://cancerdiscovery.aacrjournals.org/).

M.-H. Stern and R. Marais contributed equally to this work.

Corresponding Authors: Richard Marais, The Cancer Research UK Manchester Institute, Wilmslow Road, Manchester M20 4BX, United Kingdom. Phone: 44-161-446-3100; Fax: 44-161-918-7491; E-mail: rmarais@picr.man.ac.uk; and Marc-Henri Stern, Translational Research Department, Institut Curie, Paris 75248, France. Phone: 33-1-56-24-66-46; Fax: 33-1-56-24-66-30; E-mail: Marc-Henri.Stern@curie.fr

doi: 10.1158/2159-8290.CD-13-0330

Published OnlineFirst July 16, 2013; DOI: 10.1158/2159-8290.CD-13-0330

Class I uveal melanomas present a low risk of metastasis, whereas class II tumors are highly metastatic and are characterized by monosomy of chromosome 3 and gain of 8q. Mutually exclusive mutations in *GNAQ* or *GNA11*, the principal driver oncogenes in uveal melanoma, occur in approximately 85% of cases (5, 6), and inactivating mutations in the tumor suppressor *BAP1* occur in approximately 85% of metastatic tumors and are associated with disease dissemination (7). Recently, exome sequencing of uveal melanomas has identified recurrent mutations in *EIF1AX* and *SF3B1* (8, 9), predominantly in low-grade tumors. Somatic mutations in *SF3B1*, which encodes a component of the spliceosome, also occur in hematologic, breast, and pancreatic cancers (10–13). Mutant SF3B1 is associated with differential gene splicing in chronic lymphocytic leukemia (14), but aberrant splicing in *SF3B1*-mutant uveal melanoma has not been reported (9).

To gain insight into uveal melanoma genetics, we conducted single-nucleotide polymorphism (SNP) array analysis, whole-genome sequencing (WGS), and RNA sequencing (RNA-seq) on 12 frozen primary uveal melanoma samples. Despite its dismal prognosis, we find that uveal melanoma has a remarkably low mutation burden, and we did not observe a UVR DNA damage signature. However, we found recurrent mutations in *SF3B1* that were associated with differential alternative splicing of both coding and noncoding genes that may play a role in the etiology of this disease.

RESULTS

Our discovery cohort comprised 12 primary uveal melanoma T3–T4 tumors that represented different histologic types (one epithelioid cell, three spindle cell, and eight mixed cases) and were treated by primary enucleation (Supplementary Table S1). One case was metastatic at diagnosis and six patients subsequently developed metastases. SNP array analysis was conducted using Illumina HumanOmni2.5 SNP arrays, and whole-genome sequencing was conducted on the Illumina HiSeq 2000 platform. The whole-genome sequence coverage was >30× (Supplementary Table S2), and the data were aligned to the reference genome and duplicate reads excluded. The whole genomes were compared with their matched normal DNA to identify chromosomal translocations, short insertions/deletions (indels), and somatic single-nucleotide variants (SNV).

The SNP arrays revealed low levels of aneuploidy in 11 of the tumors and tetraploidy in tumor #7 (Supplementary Fig. S1; Supplementary Table S3). The diploid tumors presented recurrent chromosome 3 monosomy (nine tumors), losses of 1p (five tumors), 6q (three tumors), and 8p (five tumors), and gains in 6p (four tumors) and 8q (seven tumors; Supplementary Figs. S1 and S2). These aberrations are characteristic of uveal melanoma, but we also observed loss of 16q in three tumors and gain of chromosome 11 in two (Supplementary Figs. S1 and S2). The presence of two identical copies of chromosome 3 in tumor #7 suggested that chromosome 3 monosomy preceded acquisition of the tetraploid state. Tumor #7 also displayed trisomy for 1q and monosomy for 8p. Commensurate with the SNP array data, whole-genome sequencing also revealed a low level of chromosomal aberrations. We predicted two to 59 interchromosomal translocations, 0 to seven intrachromosomal translocations, no inversions, two to 25 large deletions, and 0 to five large insertions (Supplementary Fig. S2; Supplementary Table S4). Thus, the frequency of structural variations in uveal melanoma is only approximately 40% of that reported in cutaneous melanoma and only approximately 20% of that reported in acral melanoma (Fig. 1A; refs. 15, 16). It is also only approximately 10% of that we recently found in mucosal melanoma (Fig. 1A; ref. 17).

The whole-genome sequencing also revealed a very low number of SNVs. We predicted only 1629–2604 (median 2112) somatic SNVs and 47–178 (median 67) somatic short indels (Table 1). The SNV mutation rate of <1 per Mb (Table 1) is markedly lower than is seen in most other types of cancer (Fig. 1B) and significantly lower than is seen in cutaneous (~30,000 mutations/genome), mucosal (~8,000 mutations/genome), or acral (~5,000 mutations/genome) melanoma (15–17).

UVR-induced DNA damage is characterized by C>T transitions at the 3′ end of pyrimidine dinucleotides (18), a "signature" that accounts for 80% to 90% of mutations in cutaneous melanoma, and up to 60% of the mutations in acral melanoma (15, 16). Although C>T (G to A) transitions were the most common mutation in uveal melanoma, they accounted for only approximately 35% of the lesions (Fig. 1C) and were not enriched at the 3′ position of pyrimidine dimers (Fig. 1D). Thus, UVR-induced DNA damage does not seem to play a role in uveal melanomagenesis.

In line with the generally low level of mutations, we observed very few coding region mutations, predicting only 4–19 nonsynonymous SNVs per tumor; of which 92% of those tested were validated by Sanger sequencing (Supplementary Table S5). We also predicted only 0–2 coding region indels per tumor (Table 1). The only recurrent mutations were A>T, p.Q209L mutations in *GNA11* (seven tumors) and T>A/T>G, p.Q209L/P mutations in *GNAQ* (three tumors; Supplementary Table S6). We did, however, observe a small number of nonrecurrent mutations in individual genes with possible functional significance, including C>T p.P107L in *GNA15* that was coincident with A>T, p.Q209L *GNA11* in tumor #10, C>T p.G8R in *EIF1AX* in tumor #8, and *BAP1* mutations in seven tumors (Supplementary Table S6).

Critically, we also observed nonrecurrent mutations in *SF3B1* in three tumors (T>G, p.K666T: tumor #6; T>C, p.K700E: tumor #11; C>T, p.R625H: tumor #12), and although there were no chromosome losses or gains in the region containing *SF3B1* (2q33.1), these data suggested a role for *SF3B1* in uveal melanoma. We screened *SF3B1* in 105 additional consecutive archival primary uveal melanomas and detected 15 additional mutations (eight p.R625H, four p.R625C, one p.R625P, one p.R625L, one p.K666T; Supplementary Table S7). Our overall mutation rate of 15% (18/119) is similar to the rate (18.6%) recently reported for *SF3B1* mutations in uveal melanoma by whole-exome sequencing (9), but note that in addition to the R625 codon mutations reported therein, we also observed K666 and K700 codon mutations (Supplementary Fig. S3). The *SF3B1* mutations are inversely associated with chromosome 3 monosomy, and, notably, they are associated with improved progression-free and cancer survival (Supplementary Table S7; Supplementary Fig. S4).

SF3B1 encodes subunit 1 of splicing factor 3b, a component of the spliceosome, so to evaluate the effects of

Published OnlineFirst July 16, 2013; DOI: 10.1158/2159-8290.CD-13-0330

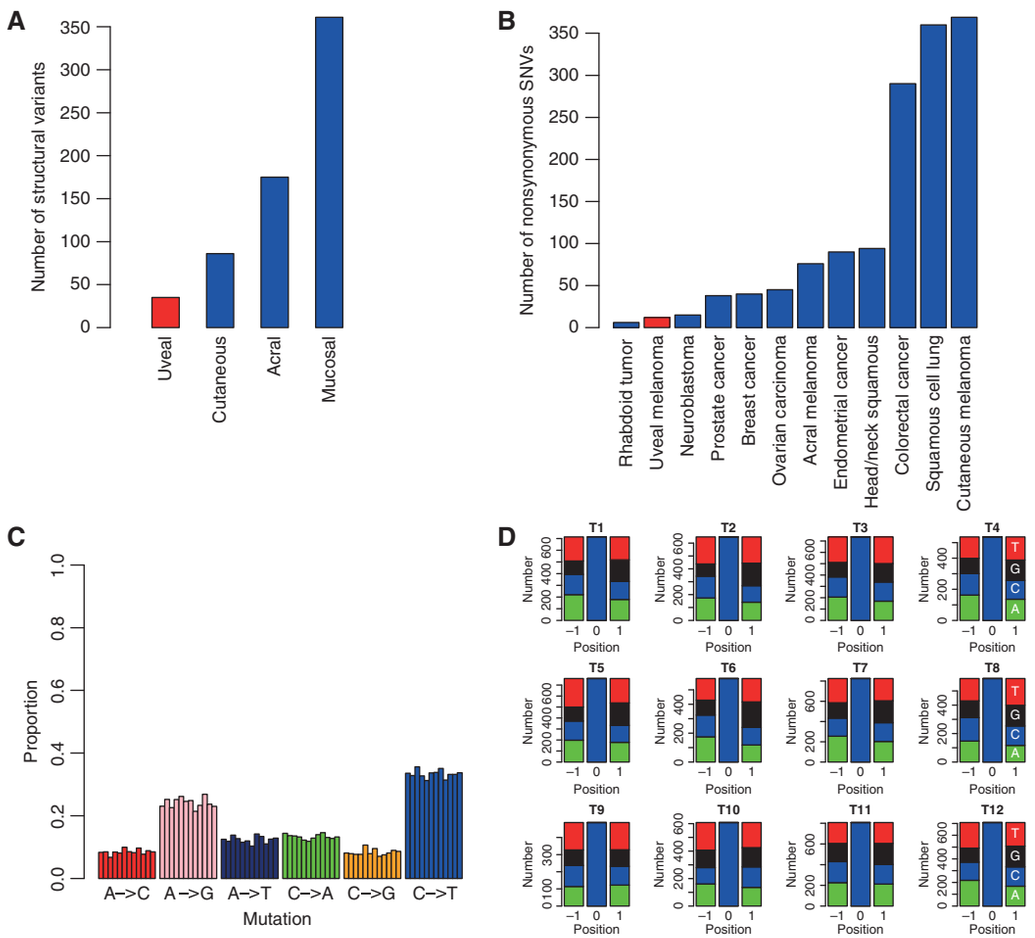

Figure 1. Somatic mutations in uveal melanoma. **A,** comparison of predicted somatic structural variation in uveal, cutaneous, acral, and mucosal melanoma subtypes. **B,** comparison of nonsynonymous point mutation rates identified from whole-genome and exome sequencing studies in various solid tumors (details and references in Supplementary Methods). **C,** proportion of predicted somatic SNVs in uveal melanoma genomes by class of mutation. **D,** frequency of bases ±1 bp of C>T/G>A mutations in the uveal melanoma genomes.

Table 1. Summary of whole-genome sequencing mutations for uveal melanoma

Tumor #	WGS SNVs	Rate per Mb	Coding region SNVs	WGS Indels	Coding region indels
1	2,301	0.80	13	178	2
2	2,084	0.73	16	62	1
3	2,207	0.77	9	52	2
4	1,712	0.60	13	49	0
5	2,604	0.91	12	93	2
6	1,778	0.62	12	47	2
7	2,531	0.89	14	89	2
8	1,768	0.62	4	48	1
9	1,629	0.57	12	56	0
10	1,934	0.68	16	72	2
11	2,566	0.90	19	102	1
12	2,229	0.78	15	86	0

NOTE: For each tumor (#1–12), the table shows the total number of predicted SNVs (WGS SNVs), the mutation rate per Mb, the number of coding region SNVs, the total number of predicted indels (WGS indels), and the number of coding region indels.

Published OnlineFirst July 16, 2013; DOI: 10.1158/2159-8290.CD-13-0330

SF3B1 mutations on uveal melanoma transcripts, we hybridized three *SF3B1*-mutated tumors and three *SF3B1*–wild-type tumors to Affymetrix Human Transcriptome Arrays (HTA2), which contain both exon and exon–exon junction probes. Three hundred twenty-five genes were predicted to be differentially expressed, with 46 genes upregulated and 279 genes downregulated in the *SF3B1*-mutant compared to the *SF3B1*–wild-type tumors (Supplementary Table S8). Gene Ontology (GO) and pathway analysis of the differentially expressed genes did not predict any significant GO term(s), and did not predict KEGG or REACTOME pathway enrichment. However, splicing level analysis predicted 130 genes that contained at least one differentially regulated exon and/or splicing pattern (Supplementary Table S9). Manual inspection of the predicted events by the GenoSplice EASANA visualization interface revealed eight high-confidence or very high-confidence events, including alternative terminal exons (four events), alternative 3′ acceptor splice sites (two events), alternative cassette exons (one event), and intron retention (one event; Table 2). Critically, six of these events (*GUSBP11*, *UQCC*, *ANKHD1*, *ADAM12*, *CRNDE*, and *ABCC5*) were also identified when we analyzed the RNA-seq data from Harbour and colleagues (Table 2).

Next, we compared the RNA-seq data from our three *SF3B1*-mutant tumors to our nine *SF3B1*–wild-type tumors. For this, we used DEXSeq, a Bioconductor package that uses generalized linear models to detect differential exon usage (19), and also MATS, which uses a Bayesian statistical framework to identify alternative splicing (20). Forty-seven genes were predicted to be differentially spliced in these two populations by at least one algorithm (Supplementary Tables S10 and S11). Strikingly, when we compared our analysis of our HTA2 and the Harbour and colleagues data with our RNA-seq analyses, three alternative splicing events involving *CRNDE*, *ABCC5*, and *UQCC*, were identified by all three analyses (Table 2). These data suggest that *CRNDE*, *ABCC5*, and *UQCC* are strong candidates for alternative splicing in *SF3B1*-mutant tumors; hence, we examined the sequencing profiles for the three genes in our RNA-seq data. We normalized the number of mapped bases for these genes and compared nucleotide coverage at each base in *SF3B1*-mutant and wild-type tumors (Fig. 2).

The profiles for *UQCC* revealed clear evidence of alternative terminal exon use in the *SF3B1*–wild-type and *SF3B1*-mutant tumors (Fig. 2A). For *CRNDE*, we observed near-uniform representation of all bases of exon 4 in the *SF3B1*–wild-type tumors, but an enrichment of the reads at the 3′ end of this exon in the *SF3B1*-mutant tumors (Fig. 2B). Finally, in ABCC5, we observed clear evidence of differential splicing of intron 8 (Fig. 2C). Critically, we detected all three of these splicing events when we analyzed the RNA-seq data from Harbour

Table 2. Alternative gene splicing associated with *SF3B1* mutations in uveal melanoma

Gene symbol	Gene name	Possible alternative event (HTA2/Geno Splice EASANA)	Harbour and colleagues RNA-Seq (GenoSplice EASANA)	Present study RNA-Seq (DEXSeq/ MATS)	qRT-PCR Validation
ABCC5	ATP-binding cassette, sub-family C (CFTR/MRP), member 5	Retention of intron 5	√	√	√
CRNDE	Colorectal neoplasia differentially expressed (non-protein coding)	Alternative acceptor site (exon 4)	√	√	√
UQCC	Ubiquinol-cytochrome c reductase complex chaperone	Alternative terminal exons	√	√	√
GUSBP11	Glucuronidase, beta pseudogene 11	Cassette exon 7	√	–	√
ANKHD1	Ankyrin repeat and KH domain containing 1	Alternative acceptors site (exon 3)	√	–	√
ADAM12	ADAM metallopeptidase domain 12	Alternative terminal exons (exon 18 vs. exon 19)	√	–	√
F8	Coagulation factor VIII, procoagulant component	Alternative first exons (exon 23 vs. exon 24)	–	–	√
GAS8	Growth arrest-specific 8	Alternative terminal exons (exon 12 vs. exon 13)	–	–	√

NOTE: For each gene indicated, the table presents the prediction of alternative splicing by the GenoSplice EASANA visualization interface in our HTA2 data and the RNA-Seq data by Harbour and colleagues (9). Also shown is the prediction of these events by DEXSeq and/or MATS in our RNA-Seq data and validation of the events by PCR.

Abbreviation: qRT-PCR, quantitative real-time PCR.

Published OnlineFirst July 16, 2013; DOI: 10.1158/2159-8290.CD-13-0330

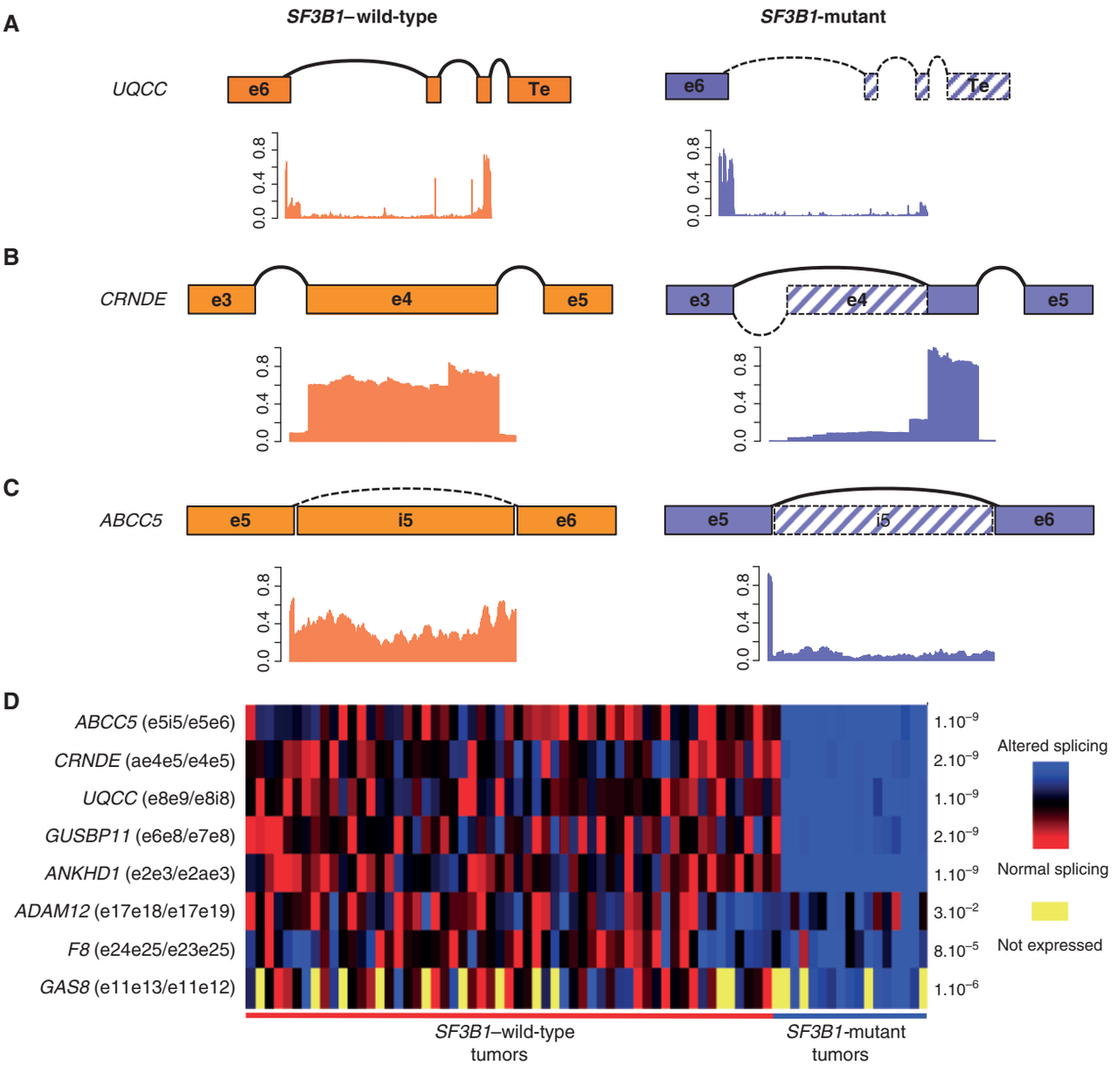

Figure 2. Alternative splicing in *SF3B1*-mutant uveal melanoma. **A–C,** plots showing normalized RNA-seq reads for *UQCC* (**A**), *CRNDE* (**B**), and *ABCC5* (**C**) in *SF3B1*-wild-type (orange) and *SF3B1*-mutant (mauve) tumors. Above the graphs we show representations of the splicing events. Exons are represented as boxes, with major splicing events indicated by the solid lines/solid boxes and minor splicing by the dotted lines/hashed boxes. Te, terminal exon; e3, e4, e5, e6: exons 3, 4, 5, 6; i5, intron 5. **D,** heatmap of the eight differentially spliced genes validated by quantitative real-time PCR in a cohort of 74 independent uveal melanoma samples (16 *SF3B1*-mutant, 58 *SF3B1*-wild-type). The brackets present the splicing form that was measured, together with exon numbers involved in each case (e, exon; i, intron; ae, alternative exon). Primer sequences used are presented in Supplementary Table S12, and *P* values (Mann–Whitney *U* test) are indicated without adjustment for the eight tests. Primary data is shown in Supplementary Fig. S6. Genes that are alternatively spliced are shown in blue; nonspliced genes are shown in red; unexpressed genes are shown in yellow. For each sample, the status of the *SF3B1* gene is indicated.

and colleagues (Supplementary Fig. S5; ref. 9), providing independent confirmation of these alternative splicing events.

Finally, to further validate our findings, we assessed alternative splicing of *GUSBP11*, *UQCC*, *ANKHD1*, *GAS8*, *F8*, *ADAM12*, *CRNDE*, and *ABCC5*, the eight genes that provided the strongest evidence of splicing, by quantitative real-time PCR in 74 independent uveal melanomas, comprising 58 *SF3B1*–wild-type tumors and 16 *SF3B1*-mutant tumors. This analysis confirmed that all eight genes were alternatively spliced in *SF3B1*-mutant tumors compared with *SF3B1*–wild-type tumors (Fig. 2D; Supplementary Fig. S6).

DISCUSSION

We describe here the first whole-genome sequencing of uveal melanoma, and our data reveal that this is a comparatively

Published OnlineFirst July 16, 2013; DOI: 10.1158/2159-8290.CD-13-0330

simple genetic disease characterized by recurrent chromosomal gains and losses and a relatively low number of SNVs and structural variants. The tumor genomes display a homogenous SNV burden, both in terms of number (1,629–2,604) and mutation class, and, notably, they do not display a canonical UVR-induced DNA damage signature at pyrimidine dinucleotides. The absence of this signature negates an obvious influence of UVR in the etiology of this disease.

We confirm that *GNAQ* and *GNA11* are the most commonly mutated driver oncogenes and that *BAP1* is the most commonly mutated tumor suppressor. In addition, we confirm *SF3B1* as recurrently mutated in 15% of cases, with a mutation hotspot at codon R625. *SF3B1* mutations have been reported in hematologic, breast, and pancreatic cancers (10–13). Intriguingly, in those cancers, codon K700 mutations predominate, whereas in uveal melanoma, R625 codon mutations predominate. This suggests either that the gene mutations have distinct etiology, so different hotspots are targeted in each disease, or that the diverse biology of the diseases favors selection of discrete mutations. Notably, in common with previous studies (8, 9), we confirm that in uveal melanoma *SF3B1* mutations are associated with better prognosis. Thus, in uveal melanoma and myelodysplastic syndrome, SF3B1 mutations are associated with improved outcome, whereas in chronic lymphocytic leukemia (CLL), *SF3B1* mutations are associated with poorer prognosis (21).

SF3B1 encodes subunit 1 of splicing factor 3b, a component of the spliceosome, a large intracellular machine that processes precursor mRNA into mature transcripts. Specifically, splicing factor 3b anchors precursor mRNA onto the spliceosome to define the splicing site. Previous studies show that spliceosomal component mutations can alter splicing within a gene, can cause intron retention, or can cause aberrant alternative splicing, affecting protein isoform balance and thereby cell proliferation and differentiation (22, 23). In CLL, *SF3B1* mutations are associated with alternative splicing at the 3′ ends of genes to generate truncated variants of the vitamin C transporter *SLC23A2*, the T-cell regulator *TC1RG1*, and the forkhead transcription factor *FOXP1*. We show that in uveal melanoma, *SF3B1* mutations are also associated with alternative splicing (Fig. 2D). We show that, in common with CLL, *SF3B1* mutations in uveal melanoma are associated with alternative splicing of the 3′ end of transcripts, for example in *UQCC*, which encodes the ubiquinol-cytochrome *c* reductase complex chaperone, a protein implicated in bone development and stature. We also see differential splicing of *ABCC5*, a multidrug resistance-associated protein that is implicated in breast cancer metastasis (24) and colorectal cancer (25). Interestingly, in uveal melanoma, we observe evidence of intron retention in *ABCC5* in the *SF3B1*–wild-type samples compared with the mutant samples, suggesting that this gene is more efficiently spliced in the *SF3B1*-mutant than wild-type tumors.

More intriguing, we show that *SF3B1* mutations are associated with cryptic alternative splicing of exon 4 of *CRNDE* transcripts (NR_034105 and NR_034106). This long noncoding RNA exists in several alternatively spliced forms and is upregulated in both solid tumors and leukemias (26, 27). *CRNDE* in general, and exon 4 in particular, is alternatively spliced in colorectal cancer and the alternative forms are thought to regulate gene expression by regulating chromatin-modifying enzymes (27, 28). We show that in uveal melanoma, mutations in *SF3B1* are associated with cryptic alternative splicing within exon 4 of *CRNDE*, and, considering the comparatively simple genetics of uveal melanoma, it will be important to determine how alternative splicing of this noncoding gene affects cellular function.

In conclusion, we show that despite its appalling prognosis, uveal melanoma is a relatively simple genetic disease characterized by recurrent chromosomal losses and gains, and a low mutational burden. We confirm that *GNAQ/GNA11* is the most commonly mutated oncogene and *BAP1* the most commonly mutated tumor suppressor. We identify *SF3B1* mutations in approximately 15% of cases and show these are associated with better prognosis, which will guide clinical management of this disease. Intriguingly, we show that *SF3B1* mutations are associated with diverse alternative splicing events, including alternative terminal exon usage, intron retention, and cryptic splicing within exons of both protein coding and noncoding genes. Future studies will focus on how these events affect uveal melanoma biology.

METHODS

Patient Cohorts

Discovery Set Twelve patients with uveal melanoma were included in the WGS study (Supplementary Table S1) from whom tumor and matched blood samples were obtained. This study was approved by the ethics committee of Institut Curie (Paris, France), and informed consent was obtained from all subjects.

Validation Set Consecutive patients diagnosed at the Institut Curie between January 2006 and December 2008 who underwent primary enucleation and with sufficient material at the Biobank were included in the validation series with exclusion of patients with metastasis at diagnosis. Patient characteristics are reported in Supplementary Table S6. The follow-up for this analysis ended in December 2012, with a median time of 38 months. During this period, 57 patients (53%) developed metastatic disease and 50 patients (47%) died. Metastatic melanoma was the cause of the death in 43 patients (40%). DNA was extracted from frozen materials or formalin-fixed paraffin-embedded (FFPE) sections. *SF3B1*, *GNAQ*, *GNA11*, and *BAP1* were sequenced by Sanger methods. Oligonucleotide primer sequences are available upon request.

DNA and RNA Extraction and Sequence Analysis

Tumor DNA and RNA were provided by the Biological Resource Center of the Institut Curie. The DNA was extracted from frozen tumor or FFPE samples using a standard phenol/chloroform procedure. The total RNA was isolated from frozen tumor samples using TRIzol reagent, and cDNA synthesis was conducted with MuLV Reverse Transcriptase in accordance with the manufacturers' instructions (Invitrogen), with quality assessments conducted on an Agilent 2100 bioanalyzer. For Sanger sequencing, genomic DNA was amplified by PCR and the products were sequenced using dye-terminator chemistry as previously described (16). Primer sequences are available upon request. Sequences were visualized using Sequencher software.

Whole-Genome Sequencing and Analysis

Extracted DNA samples were sequenced on three lanes of Illumina Hiseq2000 sequencers to produce paired-end reads of 100 bp. FASTQ files from each lane were aligned to the human reference genome (GRCh37). Data for each sample were merged and duplicate reads were marked using Picard (http://picard.sourceforge.net/). Somatic

variants were identified by comparing matched tumor and normal genomes (Supplementary Methods).

SNP Array Analysis

Genome-wide genotyping for tumor and blood DNA samples was conducted on Illumina HumanOmni2.5 SNP arrays. Raw data files were processed using GenomeStudio and somatic alterations were identified (Supplementary Methods).

RNA Extraction and Array Hybridization

Total RNA was isolated from frozen biopsy using a miRNeasy Mini Kit (Qiagen) and quality assessment was conducted using RNA 6000 Nano labchip (Bioanalyzer, Agilent) and by a Nanodrop spectrophotometer (Thermo). Total RNA integrity number values were between 7.7 and 9 (average: 8.65). Affymetrix Human Transcriptome Array 2.0 ST arrays were hybridized according to Affymetrix recommendations using the Ambion WT protocol (Life Technologies) and Affymetrix labeling and hybridization kits. One hundred nanograms of total RNA were processed in parallel with an external MAQC A RNA to control robustness of data. Labeled DNA mean yield was 7.19 μg (min: 6.27 μg; max: 7.57 μg). Affymetrix GeneChip Human Transcriptome 2.0 ST microarrays (HTA2) were hybridized with 4.7 μg of labeled DNA. Raw data, transcript data, and exon data were controlled with Expression console (Affymetrix) at the Institut Curie microarray core facility. The benefit of this array is to highlight spliced RNA isoforms using both exon and exon–exon junction probes that can measure excluded or included exons/regions.

Microarray Data Analysis

Affymetrix HTA2 dataset analysis was conducted by GenoSplice technology (www.genosplice.com and Supplementary Methods). We conducted an unpaired Student *t* test to compare gene intensities between *SF3B1*–wild-type and *SF3B1*-mutated tumors. Genes were considered significantly differentially expressed when fold change was ≥1.5 and $P \leq 0.05$ (unadjusted *P*). Analysis at the splicing level was first conducted taking into account only exon probes ("EXON analysis"; see Supplementary Methods). Results were considered statistically significant for unadjusted *P* values ≤0.05 and fold changes ≥1.5 for SPLICING PATTERN analysis and unadjusted *P* values ≤0.05 and fold changes ≥ 2.0 for EXON analysis. After bioinformatics analysis of microarray data, a manual inspection using the GenoSplice EASANA interface was conducted to select high-confident events.

RNA-Seq Analysis

RNA from the 12 tumor samples was sequenced (Supplementary Methods). Reads were aligned using Tophat (29). Differential splicing analysis between the mutant ($n = 3$) and wild-type *SF3B1* ($n = 9$) samples was conducted using DEXseq (19), and events with a false discovery rate (FDR) of <0.1 were regarded as significant. Differential splicing analysis was also conducted by MATS (20), using the mapped read bamfiles as input, and events with an FDR <0.1 were regarded as significant. The RNA-seq data from the study conducted by Harbour and colleagues (9) were downloaded from the NCBI Sequence Read Archive (http://www.ncbi.nlm.nih.gov/sra?term=SRA062359) and analyzed using the same methodology, with the exception that read lengths were trimmed to 99 bp. One of the samples described as wild-type *SF3B1* was predicted to have an *SF3B1* R625C mutation (Supplementary Fig. S7) and was designated *SF3B1* mutant for the differential splicing analysis.

Splice Variant Analysis in the Validation Series

The validation set was used to measure the predicted splice variant of eight genes using specific probes (Supplementary Table S12). A total of 1.3 ng of cDNA were analyzed in duplicate to quantify spliced and unspliced forms by real-time PCR. Forty-five cycles of quantitative PCR were conducted in 384-well plates using QuantiTect SYBR Green reagents (Qiagen) on the ABI 9700HT device. To perform the splice variant analysis, three steps were performed per gene of interest. First, C_t values were averaged per sample, then a ratio of spliced form was calculated per sample using the formula $2^{-(C_t \text{ form1 mRNA} - C_t \text{ form2 mRNA})}$. Finally, for each splicing event, a Mann–Whitney *U* test was applied between *SF3B1*-mutated and wild-type cases.

Statistical Methods

Cancer-specific survival was calculated from the date of diagnosis to death from uveal melanoma or last follow-up. Event-free survival (EFS) was calculated from the surgical resection to development of metastasis or last follow-up. Survival curves were constructed using the Kaplan–Meier method and the difference between groups was compared with the log-rank test. Chi-square and Fisher exact tests were used to determine association between variables. *P* values less than 0.05 (two-sided) were considered statistically significant.

Data Access

Whole-genome, RNA-seq, and SNP array data have been submitted to the European Genome-phenome Archive under study accession number EGAS00001000472.

Disclosure of Potential Conflicts of Interest

R. Marais has received honoraria from the speakers' bureau of Roche, has ownership interest (including patents) in The Institute of Cancer Research, and is a consultant/advisory board member of Novartis, Servier, and GlaxoSmithKline. No potential conflicts of interest were disclosed by the other authors.

Authors' Contributions

Conception and design: S.J. Furney, M. Pedersen, S. Turajlic, S. Roman-Roman, M.-H. Stern, R. Marais
Development of methodology: S.J. Furney, M. Pedersen, D. Gentien
Acquisition of data (provided animals, acquired and managed patients, provided facilities, etc.): M. Pedersen, D. Gentien, A.G. Dumont, A. Rapinat, L. Desjardins, S. Piperno-Neumann, S. Roman-Roman, R. Marais
Analysis and interpretation of data (e.g., statistical analysis, biostatistics, computational analysis): S.J. Furney, M. Pedersen, D. Gentien, A.G. Dumont, S. Piperno-Neumann, P. de la Grange, S. Roman-Roman, R. Marais
Writing, review, and/or revision of the manuscript: S.J. Furney, M. Pedersen, A.G. Dumont, L. Desjardins, S. Piperno-Neumann, S. Roman-Roman, M.-H. Stern, R. Marais
Administrative, technical, or material support (i.e., reporting or organizing data, constructing databases): D. Gentien, A.G. Dumont, L. Desjardins, R. Marais
Study supervision: M.-H. Stern, R. Marais

Acknowledgments

The authors thank Dorine Bellanger and Aurore Rampanou for technical assistance, Aurélie Kamoun for initial splicing analysis, and Odette Mariani for managing tumor samples.

Grant Support

This work was supported by Cancer Research UK (ref: C107/A10433; C5759/A12328), the Wenner-Gren Foundations, Stockholm, Teggerstiftelsen; The Harry J Lloyd Charitable Trust; and The French National Cancer Institute (INCa). A.G. Dumont is supported by the INCa grant "MeluGene."

Received July 01, 2013; revised July 12, 2013; accepted July 12, 2013; published OnlineFirst July 16, 2013.

Published OnlineFirst July 16, 2013; DOI: 10.1158/2159-8290.CD-13-0330

REFERENCES

1. Singh AD, Turell ME, Topham AK. Uveal melanoma: trends in incidence, treatment, and survival. Ophthalmology 2011;118:1881–5.
2. Singh AD, Rennie IG, Seregard S, Giblin M, McKenzie J. Sunlight exposure and pathogenesis of uveal melanoma. Surv Ophthalmol 2004;49:419–28.
3. Holly EA, Aston DA, Char DH, Kristiansen JJ, Ahn DK. Uveal melanoma in relation to ultraviolet light exposure and host factors. Cancer Res 1990;50:5773–7.
4. Tucker MA, Shields JA, Hartge P, Augsburger J, Hoover RN, Fraumeni JF Jr. Sunlight exposure as risk factor for intraocular malignant melanoma. N Engl J Med 1985;313:789–92.
5. Van Raamsdonk CD, Bezrookove V, Green G, Bauer J, Gaugler L, O'Brien JM, et al. Frequent somatic mutations of GNAQ in uveal melanoma and blue naevi. Nature 2009;457:599–602.
6. Van Raamsdonk CD, Griewank KG, Crosby MB, Garrido MC, Vemula S, Wiesner T, et al. Mutations in GNA11 in uveal melanoma. N Engl J Med 2010;363:2191–9.
7. Harbour JW, Onken MD, Roberson ED, Duan S, Cao L, Worley LA, et al. Frequent mutation of BAP1 in metastasizing uveal melanomas. Science 2010;330:1410–3.
8. Martin M, Masshofer L, Temming P, Rahmann S, Metz C, Bornfeld N, et al. Exome sequencing identifies recurrent somatic mutations in EIF1AX and SF3B1 in uveal melanoma with disomy 3. Nat Genet 2013;45:933–6.
9. Harbour JW, Roberson ED, Anbunathan H, Onken MD, Worley LA, Bowcock AM. Recurrent mutations at codon 625 of the splicing factor SF3B1 in uveal melanoma. Nat Genet 2013;45:133–5.
10. Malcovati L, Papaemmanuil E, Bowen DT, Boultwood J, Della Porta MG, Pascutto C, et al. Clinical significance of SF3B1 mutations in myelodysplastic syndromes and myelodysplastic/myeloproliferative neoplasms. Blood 2011;118:6239–46.
11. Wang L, Lawrence MS, Wan Y, Stojanov P, Sougnez C, Stevenson K, et al. SF3B1 and other novel cancer genes in chronic lymphocytic leukemia. N Engl J Med 2011;365:2497–506.
12. Biankin AV, Waddell N, Kassahn KS, Gingras MC, Muthuswamy LB, Johns AL, et al. Pancreatic cancer genomes reveal aberrations in axon guidance pathway genes. Nature 2012;491:399–405.
13. The Cancer Genome Atlas Network. Comprehensive molecular portraits of human breast tumours. Nature 2012;490:61–70.
14. Quesada V, Conde L, Villamor N, Ordonez GR, Jares P, Bassaganyas L, et al. Exome sequencing identifies recurrent mutations of the splicing factor SF3B1 gene in chronic lymphocytic leukemia. Nat Genet 2012;44:47–52.
15. Berger MF, Hodis E, Heffernan TP, Deribe YL, Lawrence MS, Protopopov A, et al. Melanoma genome sequencing reveals frequent PREX2 mutations. Nature 2012;485:502–6.
16. Turajlic S, Furney SJ, Lambros MB, Mitsopoulos C, Kozarewa I, Geyer FC, et al. Whole genome sequencing of matched primary and metastatic acral melanomas. Genome Res 2012;22:196–207.
17. Furney SJ, Turajlic S, Stamp G, Nohadani M, Carlisle A, Thomas JM, et al. Genome sequencing of mucosal melanomas reveals that they are driven by distinct mechanisms from cutaneous melanoma. J Pathol 2013;230:261–9.
18. Pfeifer GP, Besaratinia A. UV wavelength-dependent DNA damage and human non-melanoma and melanoma skin cancer. Photochem Photobiol Sci 2012;11:90–7.
19. Anders S, Reyes A, Huber W. Detecting differential usage of exons from RNA-seq data. Genome Res 2012;22:2008–17.
20. Shen S, Park JW, Huang J, Dittmar KA, Lu ZX, Zhou Q, et al. MATS: a Bayesian framework for flexible detection of differential alternative splicing from RNA-Seq data. Nucleic Acids Res 2012;40:e61.
21. Cazzola M, Rossi M, Malcovati L. Biologic and clinical significance of somatic mutations of SF3B1 in myeloid and lymphoid neoplasms. Blood 2013;121:260–9.
22. Maciejewski JP, Padgett RA. Defects in spliceosomal machinery: a new pathway of leukaemogenesis. Br J Haematol 2012;158:165–73.
23. Bonnal S, Vigevani L, Valcarcel J. The spliceosome as a target of novel antitumour drugs. Nat Rev Drug Discov 2012;11:847–59.
24. Mourskaia AA, Amir E, Dong Z, Tiedemann K, Cory S, Omeroglu A, et al. ABCC5 supports osteoclast formation and promotes breast cancer metastasis to bone. Breast Cancer Res 2012;14:R149.
25. Alhopuro P, Sammalkorpi H, Niittymaki I, Bistrom M, Raitila A, Saharinen J, et al. Candidate driver genes in microsatellite-unstable colorectal cancer. Int J Cancer 2012;130:1558–66.
26. Ellis BC, Molloy PL, Graham LD. CRNDE: a long non-coding RNA involved in cancer, neurobiology, and development. Front Genet 2012;3:270.
27. Graham LD, Pedersen SK, Brown GS, Ho T, Kassir Z, Moynihan AT, et al. Colorectal neoplasia differentially expressed (CRNDE), a novel gene with elevated expression in colorectal adenomas and adenocarcinomas. Genes Cancer 2011;2:829–40.
28. Khalil AM, Guttman M, Huarte M, Garber M, Raj A, Rivea Morales D, et al. Many human large intergenic noncoding RNAs associate with chromatin-modifying complexes and affect gene expression. Proc Natl Acad Sci U S A 2009;106:11667–72.
29. Trapnell C, Roberts A, Goff L, Pertea G, Kim D, Kelley DR, et al. Differential gene and transcript expression analysis of RNA-seq experiments with TopHat and Cufflinks. Nat Protoc 2012;7:562–78.

Published OnlineFirst July 16, 2013; DOI: 10.1158/2159-8290.CD-13-0330

AACR American Association for Cancer Research

CANCER DISCOVERY

SF3B1 Mutations Are Associated with Alternative Splicing in Uveal Melanoma

Simon J. Furney, Malin Pedersen, David Gentien, et al.

Cancer Discovery 2013;3:1122-1129. Published OnlineFirst July 16, 2013.